Remiro-Buenamañana, S.; Cabrero-Antonino, M.; Martínez-Guanter, M.; Alvaro Rodríguez, MM.; Navalón Oltra, S.; García Gómez, H. (2019). Influence of co-catalysts on the photocatalytic activity of MIL-125(Ti)-NH2 in the overall water splitting. Applied Catalysis B Environmental. 254:677-684. https://doi.org/10.1016/j.apcatb.2019.05.027

Influence of co-catalysts on the photocatalytic activity of MIL-125(Ti)-NH_2 in the overall water splitting

Sonia Remiro-Buenamañana,[1,⊥,] María Cabrero-Antonino,[2,⊥] Marcos Martínez-Guanter,[1] Mercedes Álvaro,[2] Sergio Navalón,[2,*] Hermenegildo García[1,2,3,*]*

Dr. Sonia Remiro-Buenamañana, M.Sc. Marcos Martínez-Guanter, Prof. Dr. Hermenegildo García Instituto de Tecnología Química CSIC-UPV, Universitat Politècnica de València, Consejo Superior de Investigaciones Científicas, Av. de los Naranjos s/n, 46022 Valencia, Spain

M.Sc. María Cabrero-Antonino, Prof. Dr. Mercedes Álvaro, Dr. Sergio Navalón, Prof. Dr. Hermenegildo García
Departamento de Química, Universitat Politècnica de València, C/Camino de Vera, s/n, 46022 Valencia, Spain

Prof. Dr. Hermenegildo García
Center of Excellence for Advanced Materials Research, King Abdulaziz University, Jeddah, Saudi Arabia

E-mail: sorebue@itq.upv.es, sernaol@doctor.upv.es, hgarcia@qim.upv.es

Keywords: heterogeneous photocatalysis; metal-organic frameworks; MIL-125(Ti)-NH_2; metal nanoparticles; overall water splitting

Titanium containing aminoterephthalate metal organic framework promotes the photocatalytic overall water splitting into H_2 and O_2 at a rate that depends on the presence of Pt, RuO_2 and CoOx co-catalyst. The best values of have been obtained for the MIL-125-NH_2 material that contains Pt and RuO_2, reaching a production of 218 and 85 μmol/$g_{photocatalyst}^{-1}$ at 24 h for H_2 and O_2, respectively.

1. Introduction

In the context of the transition from fossil to renewable fuels, there is much interest in the production of solar fuels by photocatalysis.[1-7] Although TiO_2 and other wide bandgap metal oxides are efficient photocatalysts under UV irradiation,[8-9] the solar spectrum reaching the Earth surface contains mainly visible and near-infrared photons and the response of these materials to these wavelengths is usually negligible. Different strategies have been developed to introduce visible light photoresponse in metal oxide semiconductors, but there is still a need for exploring different materials.[9-10]

Among the photocatalysts alternative to metal oxides, metal-organic frameworks (MOFs) have attracted much current interest.[11-15] MOFs are crystalline porous materials in where the lattice is constituted by nodes of a transition metal ion or a cluster of a few metal ions that are held in place by rigid bi- or multipodal organic linkers, typically aromatic polycarboxylates.[16-20] MOFs offer as photocatalysts a series of advantages including a wide flexibility in the composition, high surface area and porosity, a large degree of design and the possibility to incorporate guests that can act as co-catalysts. [14 16, 21] As an example, the presence of amino substituents in the aromatic linker has been used to expand the photoresponse of MOFs into the visible region,[22-24] while the intimate contact between linkers and metal nodes is responsible in many cases for an efficient electron transfer from excited organic linker to the metal nodes.[25] Due to the combination of these favorable features, MOFs have been reported among the most efficient visible light photocatalysts for hydrogen generation and photocatalytic CO_2 reduction, among other reactions.[14, 26-28]

In the vast majority of the reported examples in the use of MOFs for hydrogen generation upon visible light excitation have employed sacrificial electron donors, there being only a few precedents on the use of MOFs for overall water splitting.[11, 13-14] Since photon absorption generates electrons and holes that have to be consumed at the same rate, the presence

of electron donors quenching the holes, decouples the reductive hydrogen generation process from hole consumption. Accordingly, in the presence of good electron donor agents, the highest efficiency for hydrogen generation can be reached.[29-30] However, when considering the real application of hydrogen generation from water, the two processes, hydrogen generation and oxygen evolution from water have to take simultaneously place. Since oxygen evolution from water is a four electrons, four protons process, it is thermodynamically and kinetically the limiting step.[8, 31-32] There are only a few precedents describing photocatalytic oxygen evolution using MOFs as photocatalyst[33] and photocatalytic overall water splitting promoted by MOFs has been rarely reported,[34-35] in spite of the large number of published articles using these materials for photocatalytic hydrogen generation articles.

In view of the scarcity of reports describing the overall water splitting by MOFs, this area remains still largely unexplored. This situation sharply contrasts with the vast number of studies on the photocatalytic hydrogen generation by MOFs.[11, 13, 33] Therefore, there is a need to provide additional information regarding the possibility to conduct overall water splitting by MOFs.

The present manuscript reports the influence of various co-catalysts on the overall water splitting using MIL-125(Ti)-NH_2 as solar light photocatalyst. It will be shown that the photocatalytic activity largely depends on the presence of co-catalysts, the highest efficiency being reached when two complementary co-catalysts to manage the transfer of electrons and holes, are simultaneously present in the material.

2. Experimental Section

2.1. Materials

All the reagents employed in this work were of analytical or HPLC grade and supplied by Sigma-Aldrich.

2.2. Catalyst Preparation

Synthesis of MIL-125(Ti)-NH_2. MIL-125(Ti)-NH_2 was prepared following previously reported procedures.[36-38] Briefly, 2-aminoterephthalic acid (1.43 g, 7.9 mmol) was dissolved in anhydrous N,N-dimethylformamide (DMF, 20 mL), then, anhydrous methanol (5 mL) was added to the flask and the system sonicated for 20 min. The reaction mixture was transferred to a Teflon-lined autoclave (50 mL) before titanium isopropoxide (1.36 g, 4.8 mmol) was added. The autoclave was sealed and heated at 110 °C for 72 h. After cooling the system to room temperature, the resulting precipitate was filtered, washed with DMF at room temperature for 12 h and, then, washed with DMF at 120 °C for 12 h. This washing procedure was repeated using methanol as solvent. Finally, the solid was recovered by filtration and dried in an oven at 100 °C.

Synthesis of MIL-125(Ti). MIL-125(Ti) was prepared following the procedure described by Se-NaKim.[39] Briefly, titanium isopropoxide (9 mmol) and 1,4-benzene dicarboxylic acid (15 mmol) were added to a mixture of DMF and methanol (9:1; 50 mL) in a Duran bottle (150 mL) and the system sonicated for 20 min. Subsequently, the mixture was heated in oven at 150 ºC for 16 h. After cooling to room temperature, the resulting precipitate was filtrated and washed twice with DMF and methanol as in the case described for MIL-125(Ti)-NH_2. Finally the resulting solid was dried at 150 °C overnight under vacuum.

Preparation of metal nanoparticles (MNPs, M: Pt, CoOx and RuOx) on MIL-125(Ti)-NH_2. MNPs were deposited in the previously formed MIL-125(Ti)-NH_2 solid using the photodeposition method.[40] Briefly, MOF (50 mg) was dispersed in the corresponding solvent (18 mL) using a quartz tube. For the preparation of Pt, CoO_x and RuO_x NPs, a mixture of Milli-Q water (13 mL) and MeOH (5 mL) as sacrificial agent was employed. In the case of Pt-RuO_x-MIL-125(Ti)-NH_2 water (18 mL) was employed as solely solvent. After dispersion of the MOF in the appropriate solvent, the metal salt precursor dissolved in water (2 mL) was added and the system purged with Ar for 20 min. The mixture was subsequently irradiated with UV-Vis light lamp for 4 h. The solid obtained was filtered, washed with water and dried in oven at 100 °C overnight. The monometallic cobalt and ruthenium NPs deposited on MIL-125(Ti)-NH_2 solid the samples were further oxidized on purpose at 180 ºC for 2 h in an oven under ambient conditions.

2.3. Catalyst Characterization

Powder X-ray diffractograms (PXRD) were recorded using a Philips XPert diffractometer equipped with a graphite monochromator (40 kV and 45 mA) employing Ni filtered CuKα radiation. The morphology and composition of the MOF samples were characterized using a scanning electron microscope (SEM, Zeiss instrument, AURIGA Compact) coupled with a EDX detector. Scanning transmission electron microscopy images in dark field (DF-STEM) were recorded on a JEOL JEM2100F instrument operating at 200 kW. MNP size distribution was estimated by measuring more than 300 particles from the sample. Isothermal nitrogen adsorption measurements were carried out using an ASAP 2010 Micromeritics device. X-ray photoelectron spectra (XPS) were collected on a SPECS spectrometer with a MCD-9 detector using a monochromatic Al (Kα= 1486.6 eV) X-ray source. Spectra deconvolution was performed after Shirley subtraction of background with the CASA software using the C 1s peak at 284.4 eV as binding energy reference. Inductively coupled

plasma-atomic emission spectroscopy (ICP-AES) analysis was used to determine the metal content of the catalyst after dissolving it in concentrated nitric acid. FTIR spectra were recorded on compressed powders using a Bruker spectrophotometer in an attenuated total reflectance (ATR) cell.

2.4. Photocatalytic Experiments

2.4.1. Photocatalytic Overall Water Splitting Tests

The photocatalyst sample was sonicated for 10 min in the appropriate amount of Milli-Q water (optimized concentration 1 mg of photocatalyst per mL of water) to obtain a good dispersion of the photocatalyst. The suspension was placed in a quartz reactor and the system was purged for 1 h under argon to evacuate oxygen from the solution and the atmosphere. The suspension was stirred at room temperature and irradiated with a 300 W Xenon lamp while maintaining stirring. The gases evolved were analyzed from the head space connecting directly the reactor to an Agilent 490 Micro GC system (Molsieve 5 Å column using Ar as carrier gas) without manual handling. The temperature of the reactor was monitored and the pressure was analyzed by means of a manometer.

2.4.2 Monochromator experiments

The Pt-RuO_2-MIL-125(Ti)-NH_2 (20mg) photocatalyst was suspended in Milli Q H_2O (20mL), the solution was treated as described in section 2.4.1. The suspension was subsequently excited with a 150 W Xenon lamp through a CzernyeTurner monochromator (PTI model 101). The incident power density was calculated using a Newport (818-UV-L) calibrated photodiode. The sample was irradiated at the following

wavelengths: 350 nm (2.358 W/m^2), 400 nm (9.906 W/m^2) and 450 nm (16.943 W/m^2). Quantum yields were calculated according to Equation 1 and Equation 2.

$$\phi = \frac{\text{number photons emitted}}{\text{number photons absorbed}} \text{ x } 100 = \frac{\text{number molecules } H_2 \text{ x } 2}{\text{number photons incidents}} \qquad \text{Equation 1}$$

$$\text{Number photons incidents} = \frac{E \text{ x } \lambda \text{ x Radiated Area}}{c \text{ x } \hbar} \quad \text{Radiated Area} = \frac{\pi \text{ x } d^2}{4} \qquad \text{Equation 2}$$

2.4.3 Quenching experiments using MeOH or $Ce(NO_3)_4$

The photocatalyst was suspended in an aqueous solution (V_{total} = 20 mL) containing either MeOH (20%) as donor or $Ce(NO_3)_4$ (0.01 mM) as electron acceptor, and the samples were irradiated in a quartz reactor under the same Xenon light source. H_2 and O_2 evolution were monitored using a Micro GC.

2.4.4 Labelled $H_2{}^{18}O$ experiment

This experiment was carried out using an especially designed small quartz reactor (V_{max} = 2 mL), Pt-RuO_2-MIL-125(Ti)-NH_2 (5mg) was introduced in the reactor and labelled $H_2{}^{18}O$ (500 μL) was subsequently introduced. The system was purged with helium for 5 minutes and the mixture was irradiated using a Xe lamp. Gases were analyed in a GC-MS (5973N-6890N) Agilent spectrometer equipped with TRB-5MS column (5% phenyl, 95% polymethylsiloxane, 30 m, 0.25 mm × 0.25 μm, Teknokroma).

2.4.5 Experiment under natural Sunlight irradiation

The reactor was set in the building roof on a sunny spring day (geographic coordinates: 39.478766/-0.339703) with a highest ambient temperature of 30 °C and an ambient relative humidity of 85 %. The mixture was stirred under the specified conditions and samples were analyzed by a micro gas chromatograph.

3. Results and Discussion

3.1. Catalyst preparation and characterization

The purpose of the present study is to obtain data of the photocatalytic overall water splitting of MIL-125(Ti)-NH_2 having co-catalysts to promote simultaneous hydrogen and oxygen evolution. For the sake of sample characterization, MIL-125(Ti) was also prepared. In agreement with previous reports,[41] Figure 1a shows that MIL-125(Ti) and MIL-125(Ti)-NH_2 are isostructural crystalline solids. In addition, the titanium metal content determined by ICP-OES of a previously acid digested MIL-125(Ti) or MIL-125(Ti)-NH_2 sample agrees with the theoretical formula of these MOFs, either $Ti_8O_8(OH)_4BDC_6$ or $Ti_8O_8(OH)_4(NH_2\text{-}BDC)_6$, respectively, confirming the high crystallinity of the solids. Termogravimetric analysis of the MIL-125(Ti)-NH_2 sample confirm the thermal estability of the sample up to 300 ºC and allow also to corroborate the experimental amount of titanium of the sample (22.5 %) in good agreement with the theorethical one (23 % for the $C_{48}H_{34}N_6O_{36}Ti_8$) (Figure S1). The presence of the amino group in the MIL-125(Ti)-NH_2 solid was assessed by observing its characteristic N-H (3,300, 1,610 and 760 cm^{-1}) and C-N (1,255 cm^{-1}) FT-IR vibration bands that do not appear in the MIL-125(Ti) sample (Figure S2). XPS of individual atoms (C1s, O1s, Ti2p and/or N1s) present in the MIL-125(Ti)-NH_2 material (Figure S3) in agreement with the literature.[38, 42-43]

As already known, MIL-125(Ti) absorbs light in the UV region, while the presence of $–NH_2$ substituent in MIL-125(Ti)-NH_2 expands its absorption towards the visible by introducing a new electronic transition involving the lone electron pair region of the nitrogen atoms.[27] Figure 1b presents the diffuse reflectance UV-Vis spectra of series of MIL-125(Ti) materials under study. As it can be observed in this Figure, MIL-125(Ti) and MIL-125(Ti)-NH_2 exhibit a more intense band in the UV region with a maximum of 280 nm that is ascribed to the

Ti-O ligand to metal charge transfer transition. In the case of the MIL-125(Ti)-NH_2, another absorption band with maximum around 380 nm is recorded. This band is associated to the electron transfer from the aminoterephthalate ligand to the $Ti_8O_8(OH)_4$ cluster.

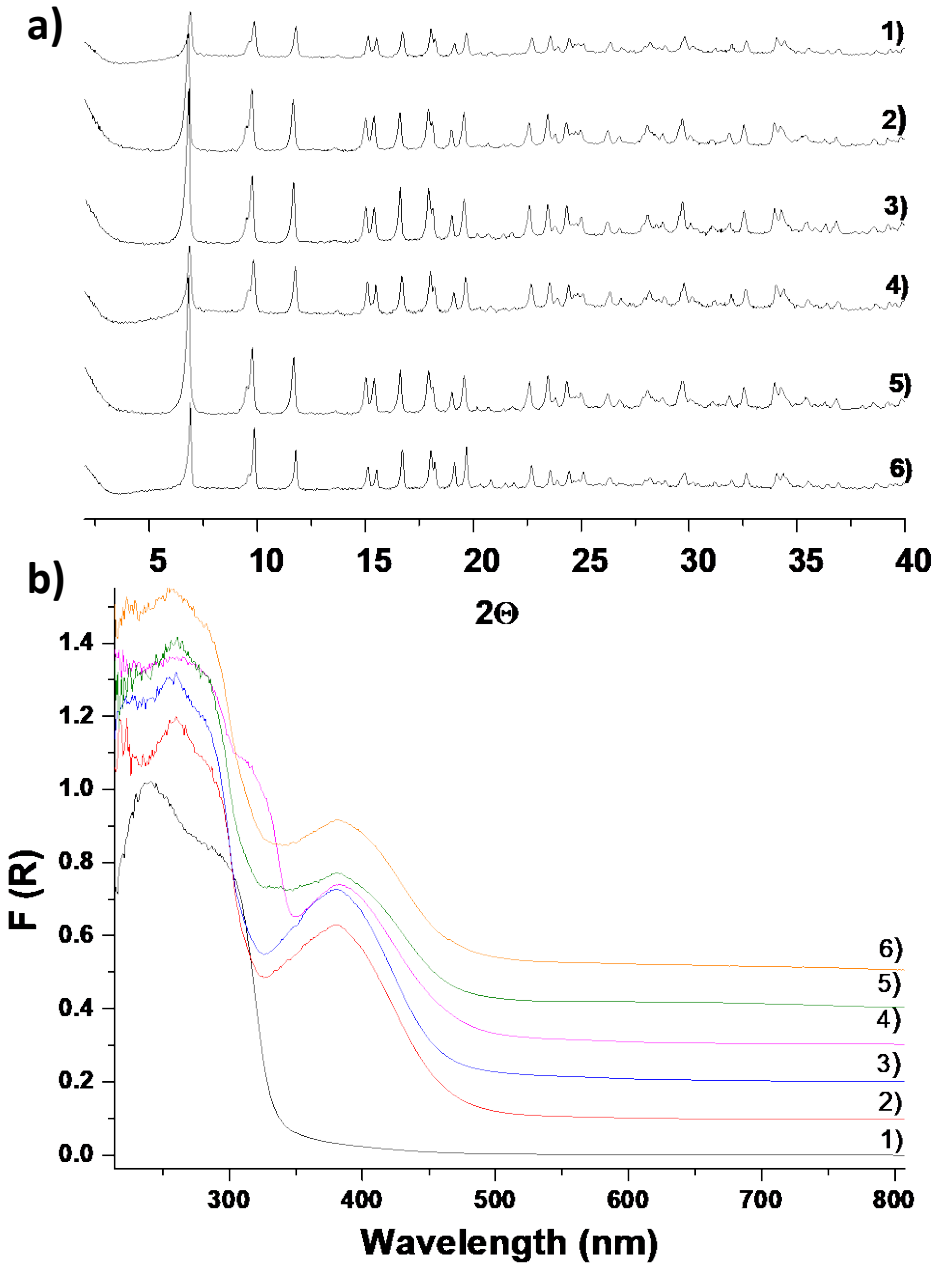

Figure 1. XRD (a) and (b) DR-UV spectra of the MIL-125(Ti)-NH_2 series presented in this work. 1) MIL-125(Ti), 2) MIL125(Ti)-NH_2, 3) CoO_x-MIL125(Ti)-NH_2, 4) Pt-MIL-125(Ti)-NH_2, 5) RuO_x-MIL125(Ti)-NH_2, 6) Pt-RuOx-MIL125-NH_2.

The morphology (Figure S4) and the composition of these two materials have been assessed by SEM measurements coupled to EDX measurements (Figures S5-S6). The porosity

of the materials was assessed by performing isothermal N_2 adsorption measurements. Regardless space needed for accommodation of the amino group in the MIL-125(Ti)-NH_2 material a high BET surface area and pore volume of 1,200 $m^2\ g^{-1}$ and 0.55 g cm^{-3}, respectively, were obtained.

Co-catalysts were introduced on the material to determine the influence of the nature of these guests on the efficiency of the overall water splitting. MNP deposition on MIL-125(Ti)-NH_2 solid was performed by irradiating the material with UV-Vis light to generate electron-hole pairs in the absence Pt-RuO_2 or in the presence of MeOH as sacrificial agent (RuO_2 and CoO_x). Figure 1a shows that the crystal structure of the MIL-125(Ti)-NH_2 remains unaltered upon photodeposition of the co-catalysts. The absence of diffraction peaks characteristic of the metal or metal oxide NPs indicates the good dispersion and/or small supported MNPs. This fact has been confirmed by means of TEM measurements (Figure 2).

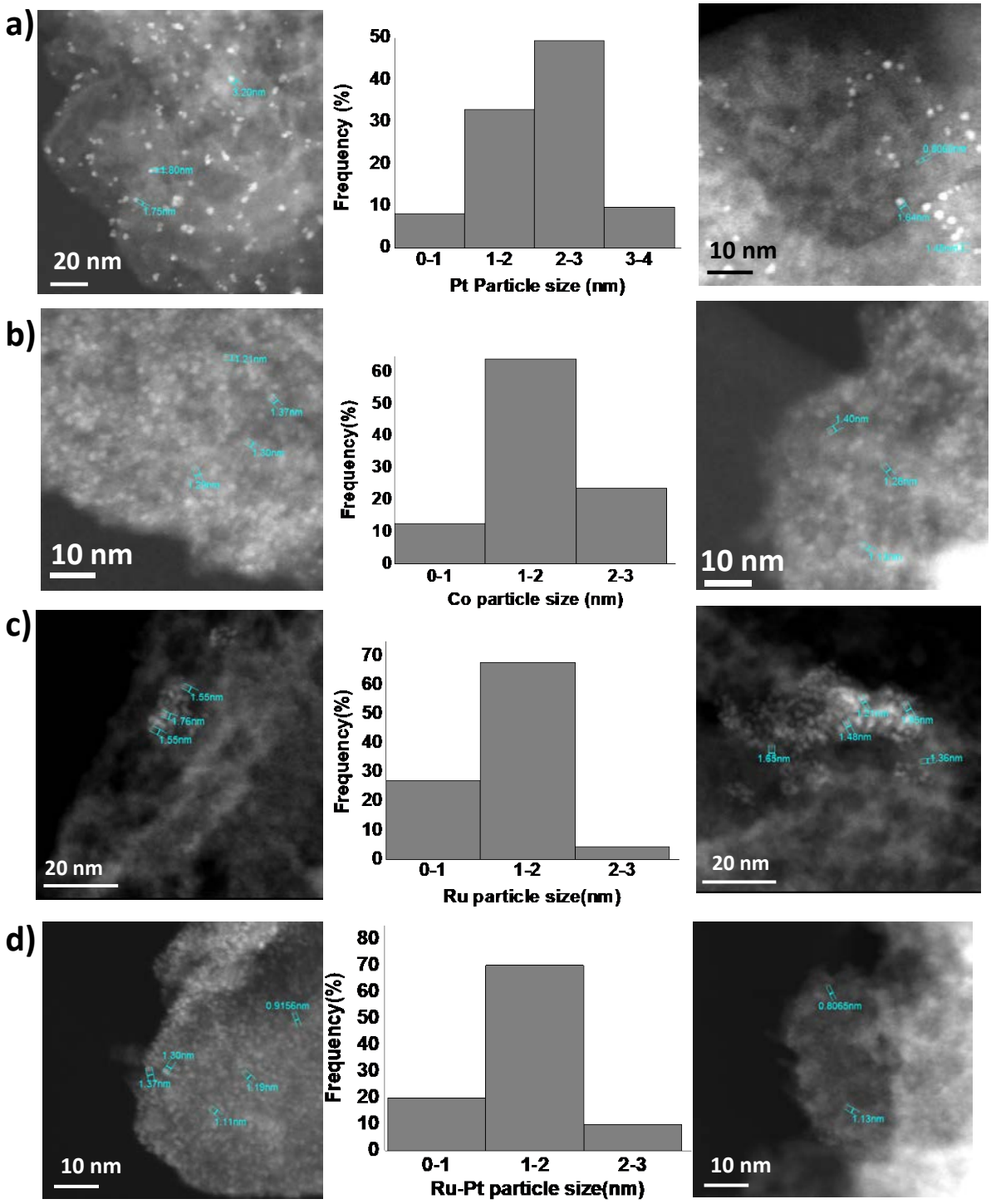

Figure 2. DF-STEM images and histogramas of metal particle size distribution of Pt-MIL-125(Ti)-NH_2 (a), CoO_x-MIL-125(Ti)-NH_2 (b), RuO_x-MIL-125(Ti)-NH_2 (c) and Pt-RuO_x-MIL-125(Ti)-NH_2 (d).

Table 1 summarizes the metal content, metal or metal oxide particle size distribution and standard deviation of the prepared catalyst. In general, the average particle size of the photodeposited co-catalyst NPs on MIL-125(Ti)-NH_2 is lower than 3 nm, being compatible with the internal location of these NPs. The composition of these small MNPs has been confirmed by performing selected area EDX analyses of individual MNPs on the as-prepared materials (Figure S7). SEM-EDX measurements revealed the good dispersion of the different elements (Figures S8-S11). XPS allows to detected all the expected elements (C, O, N, Ti) of the different samples as well as to confirm the predominant reduction form of Pt(0) NPs and oxidized CoO_x NPs (Figures S12-S15). Ruthenium nanoparticles, however, overlaps with C1s binding energy although considering that after the photodeposition the sample is treated at 180 ºC for 2 h in an oven under ambient conditions it is likely assume that are partially oxidized in the form of RuO_x. (Figure S14). As it will be commented below, somewhat different co-catalyst loadings were achieved by photodeposition. However, this method of co-catalyst formation was preferred, since this method ensures the formation of the co-catalyst NPs at those locations of the crystal were electrons (Pt) or holes (CoO_x and RuO_x) are preferentially located.[26] The loading of these co-catalysts are given in Table 1.

Table 1. List of MIL-125(Ti)-NH_2 photocatalysts employed in this study for the overall water splitting.[a,b]

Photocatalyst	Metal Content (wt%)[c]	Average particle size (nm) and standard deviation (nm) of fresh samples	Average particle size (nm) and standard deviation (nm) of used samples
Pt-MIL-125(Ti)-NH_2	0.20	2.1±0.50	2.3±0.51
CoO_x-MIL-125(Ti)-NH_2	0.95	1.6±0.45	1.8±0.49
RuO_X-MIL-125(Ti)-NH_2	0.23	1.3±0.51	1.3±0.52
Pt-RuO_x-MIL-125(Ti)-NH_2	0.12(Pt)-0.24(Ru)	1.4±0.44	1.5±0.53

[a)] Isothermal nitrogen adsorption measurements allowed to estimate a BET surface area and pore volume of 1.200 $m^2\ g^{-1}$ and 0.55 g cm^{-3}, respectively; [b)] The same batch of the MIL-125(Ti)-NH_2 has been employed to prepare this sample; [c)] Determined by ICP-AES after acid digestion of the solid samples.

3.2. Photocatalytic Overall Water Splitting Experiments

Considering the known influence of the amino substitution on the terephthalate ring on the visible light absorption, MIL-125(Ti)-NH_2 was selected as photocatalyst to determine its performance to promote the overall water splitting under simulated sunlight irradiation as a function of the nature of co-catalyst. Previous calculations have proposed that the highest occupied crystal orbital (HOCO) in MIL-125(Ti)-NH_2 is located at the organic linker and the lowest unoccupied crystal orbital (LUCO) at the Ti 3d-orbitals.[44] Accordingly, it is expected that upon photon absorption, an efficient electron transfer from the terephthalate ligand to the Ti^{4+} cation can occur, as it has also been proposed based on transient absorption spectroscopy.[45] In agreement with these proposals, EPR measurements have shown that photoexcitation of MIL-125(Ti)-NH_2 results in the formation of Ti^{3+} species.[46] Moreover, the energy values of the valence and conduction bands in MIL-125(Ti)-NH_2 (see Table 2) would, in principle, allow this material in the charge separated state to perform the overall water splitting. [34, 47] Thus, the bottom level of the conduction band is more negative than the reduction potential of the H^+/H_2 couple (E^0_{red} 0 V vs NHE), and the top level of the valence band more positive than the oxidation potential of the O_2/H_2O redox pair (+1.23 V vs NHE). In accordance with previous reports, [34, 47] the estimated band gap of the MIL-125(Ti)-NH_2 material is around 2.45 eV, therefore, it also meets the requirement of having a band gap higher than the necessary 2.3 eV to permit the reaction. Table 2 summarizes the thermodynamic data.

Table 2. HOCO and LUCO energy values and bandgap energy for MOFs related to the MIL-125 series.[34, 47]

Material	HOCO [eV]	LUCO [eV]	Band Gap [eV]
MIL-125(Ti)	2.40	-1.40	3.80
MIL-125(Ti)-NH_2	2.40	-0.05	2.45

As already mentioned, most of the literature precedents are focused on the evolution of one of the semi-reactions, particularly hydrogen.[14-15, 48] Thus despite their known sensitivity to

pH, MOFs have proven its capability to generate hydrogen or oxygen in the presence of sacrificial electron donors and electron acceptors.[49] There are only two examples regarding the overall water splitting utilizing MOFs as photocatalyst in the literature, both by Huang, Liu and colleagues, reporting the use of an aluminium based MOF derived from 2-aminoterephthalic acid (Al-NH_2BDC MOF)[35] and also MIL-125(Ti) doped with CoPi (Pi phosphate) and Pt.[34] To the best of our knowledge there are no examples regarding the use of MIL-125Ti)-NH_2 for the overall water splitting.

Apart from different LUCO and bandgap energy values, the main advantage of MIL-125-NH_2 against MIL-125 is the extended absorption in the visible region what is extremely important in solar photocatalysis. For their use in the overall water splitting, MIL-125-NH_2 was functionalized by photodeposition[40] with co-catalysts, namely Pt, CoO_x, RuO_x and a bimetallic Pt-RuO_x material.[26] The roles of co-catalysts are to improve the efficiency of charge separation and to act as active sites for oxygen and hydrogen evolution.[34] Numerous studies have shown that Pt NPs are the preferred active sites for H_2 evolution,[26] while O_2 evolution reaction is commonly catalyzed by RuO_2[50] or oxidized cobalt NPs.[50-51]

In a preliminary experiment, the photocatalytic overall reaction was performed over as-synthesized MIL-125-NH_2 to evaluate the performance of the semiconductor without any co-catalyst in the system. It was observed that H_2 and O_2 gases were generated in a *quasi*-stoichiometric ratio resulting in 48 and 27 $\mu mol \cdot g^{-1}_{photocatalyst}$ of H_2 and O_2, respectively, in 21 h (Figure 3a). Control experiments in the dark showed no H_2 and O_2 evolution (data not shown). The concentration of the heterogeneous photocatalyst was optimized keeping constant irradiation conditions (Figure 3b). As it can be seen there, lower catalyst concentrations (10 or 5 $mg_{photocatalyst}$·20 mL of water) resulted in higher H_2 or O_2 production per weight of MOF spent in the reaction. However, these small amounts of MIL-125(Ti)-NH_2 result in lower oxygen evolution that would be affected by larger experimental errors and, therefore, were not chosen.

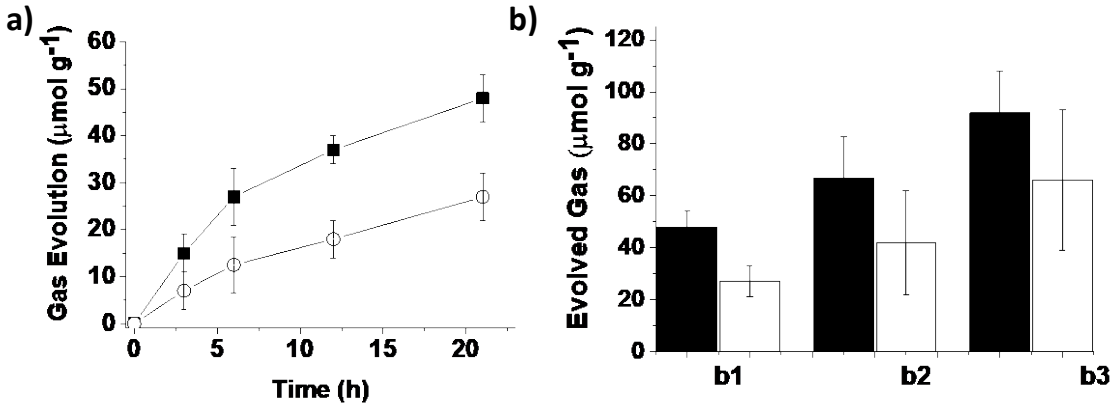

Figure 3. a) Photocatalytic H_2 and O_2 evolution reaction over MIL-125(Ti)-NH_2. b) Photocatalytic gas evolution MIL-125(Ti)-NH_2 using different photocatalyst concentrations: Catalyst concentration of 20 mg/20 mL (a, b1), 10 mg/20 mL (b2), 5 mg/20mL (b3). Legend: H_2 (black symbols) and O_2 (white symbols) Reaction conditions: light source: UV-Vis Xe lamp (150 mW×cm^{-2}), H_2O (20 mL), photoreactor volume (51 mL), temperature (35 °C).

To study the effect of co-catalyst deposition on the photocatalytic water splitting, cobalt oxide NPs were photodeposited onto pristine MIL-125(Ti)-NH_2. As it can be observed in Figure 4a, this CoO_x-MIL-125(Ti)-NH_2 photocatalyst is also able to promote overall water splitting with a maximum H_2 and O_2 production of 147 and 61 μmol·g$^{-1}_{photocatalyst}$, respectively, in 21 h. Thus, loading CoO_x NPs in less than 1 % in MIL-125(Ti)-NH_2 increases by three-fold the gases evolved compared to the pristine MIL-125(Ti)-NH_2. This improvement in the activity of the photocatalyst reflects the positive effect of cobalt oxide as co-catalyst to lower the activation energy.

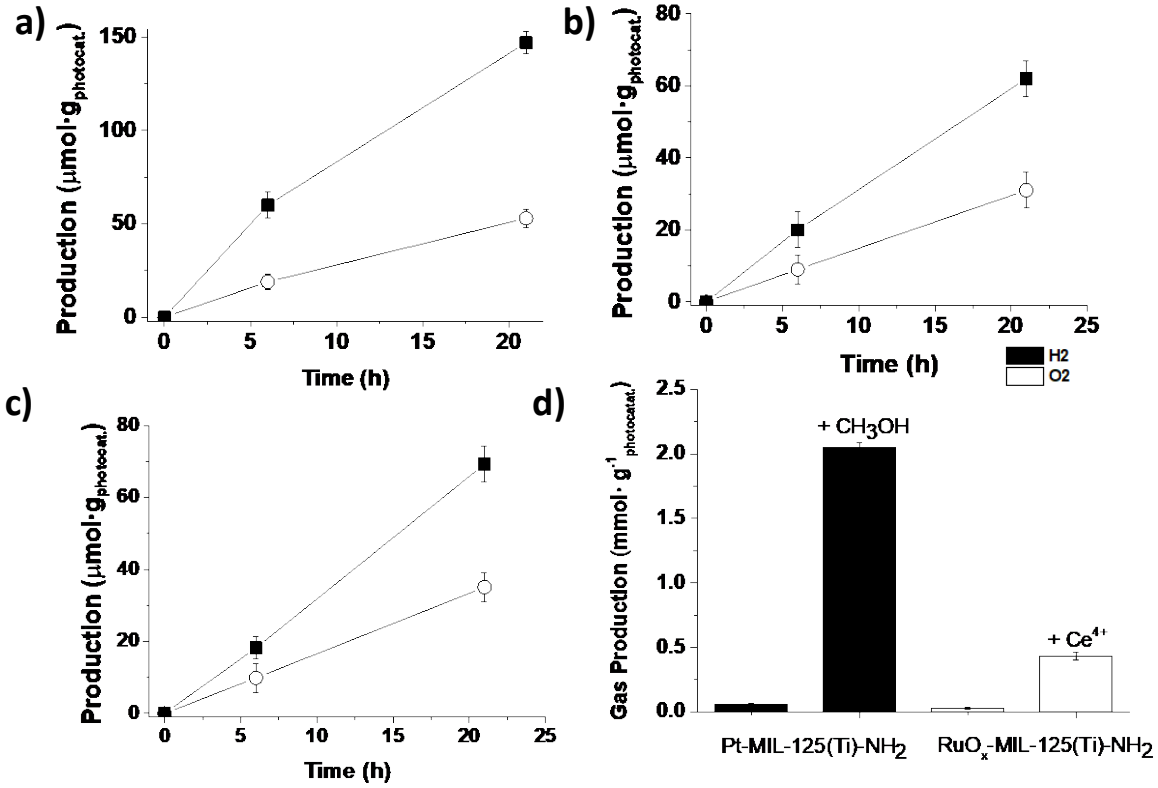

Figure 4. Photocatalytic H_2 and O_2 evolution per gram of CoO_x-MIL-125(Ti)-NH_2 (a), Pt-MIL-125(Ti)-NH_2 (b) and RuO_x-MIL-125(Ti)-NH_2 (c). Comparison of the photocatalytic H_2 production for Pt-MIL-125(Ti)-NH_2 (black bars) and O_2 production for RuO_x-MIL-125(Ti)-NH_2 (white bars) in the absence or in the presence of indicated sacrificial agents. Reaction conditions: Photocatalyst (20 mg /20 mL Milli Q-H_2O), UV-Vis Xe lamp (150 mW×cm^{-2}), temperature 35 ˚C.

Besides cobalt oxide, the influence of the presence of Pt NPs on the overall water splitting was also investigated. Pt-MIL-125(Ti)-NH_2 was characterized and tested for the overall water splitting under the optimal conditions commented above. The average Pt NP particle size was 2.2 nm that is compatible with the internal location of the NPs prepared by photodeposition. Figure 4b depicts the gas evolution and the time profiles for the photocatalytic overall water splitting over Pt-MIL-125(Ti)-NH_2. There was also improvement in the values with respect to the blank MIL-125(Ti)-NH_2 obtaining in this case up to 62 µmol g^{-1} of H_2 and the stoichiometrically generated O_2 (31 µmol g^{-1}). The enhancement of the reaction is smaller than the one measured for cobalt oxide as co-catalyst. When comparing the performance of

both CoO_x and Pt NPs as co-catalysts, it should, however, be reminded that the loading of cobalt oxide and Pt NPs in weight percentage is not exactly coincident and it is likely that other co-catalyst loadings could have given different enhancements of the photocatalytic activity. The most conclusive point was that both co-catalyst enhance the photocatalytic activity for overall water splitting respect to the pristine MIL-125(Ti)-NH_2 material.

A third co-catalyst tested for the overall water splitting was ruthenium oxide, also a typical co-catalyst for oxygen evolution.[50] An enhancement in the photocatalyst activity for overall water splitting similar to that measured for Pt NPs was observed upon photodeposition of RuO_2. H_2 and O_2 generation values were 70 and 35 μmol, respectively (Figure 4c) when Ru-MIL-125(NH_2) was used as photocatalyst. When making the comparison, it should be commented again, the impossibility to prepare by photodeposition samples with exactly the same atomic loading of different metals or metal oxides per weight of MIL-125(Ti)-NH_2.

To evaluate the reduction and oxidation semi-reactions independently, the photocatalytic gas evolution measurements were carried out in the presence of methanol as electron donor in case of Pt-MIL-125(Ti)-NH_2 and cerium ammonium nitrate as electron acceptor for RuO_x-MIL-125(Ti)-NH_2. The results, depicted in Figure 4d, clearly demonstrated that the efficiency of H_2 and O_2 evolution increases considerably in the presence of the appropriate sacrificial agent. These results are in good agreement with the literature that shows that H_2[14] or O_2[52] evolution in aqueous suspensions reaches the maximum values when sacrificial agents are present in the medium quenching efficiently holes and electrons, respectively. In this way, a remarkable increase of the produced gases is achieved in the presence of complementary sacrificial agents, reaching values of 2 mmol $H_2 \cdot g_{photocatalyst}^{-1}$ when MeOH is added to the Pt-MIL-125(Ti)-NH_2 photocatalyzed reaction, and about 0.5 mmol of $O_2 \cdot g_{photocatalyst}^{-1}$ when $Ce(NO_3)_4$ is present in the reaction photocatalyzed by RuO_2-MIL-125(Ti)-NH_2.

To check whether the photocatalytic activity for overall water splitting improves in the presence of two complementary photocatalysts, a MIL-125(Ti)-NH_2 containing both Pt and

RuOx NPs was prepared. The results presented in Figure 5a and show that the water splitting activity of the MIL-125(Ti)-NH_2 containing both Pt and RuOx co-catalyst is the highest of the series (Figure 5b) reaching values of H_2 and O_2 production of 218 and 85 $\mu mol \cdot g_{photocatalyst}^{-1}$, respectively at a reaction tempeature of 35 ºC. An analogous experiment working at 10 ºC results in a H_2 and O_2 production of 88 and 38 $\mu mol \cdot g_{photocatalyst}^{-1}$, respectively (Figure S16). The lower than stoichiometric O_2 production observed in the measusrement could indicate alternative ways of hole consumption and/or the reaction of some percentage of nascent O_2 with Ru co-catalyst, other MOF components or electrons.

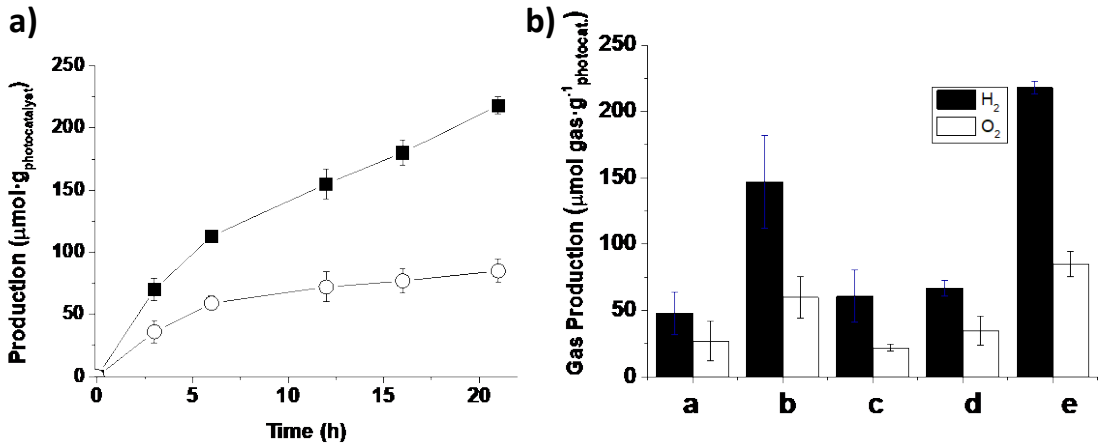

Figure 5. a) Overall water splitting using Pt-RuO_x-MIL-125(Ti)-NH_2 as photocatalyst. b) Values of H_2 and O_2 production for the photocatalytic overall water splitting using MIL-125(Ti)-NH_2 (a), CoO_x-MIL-125(Ti)-NH_2 (b), Pt-MIL-125(Ti)-NH_2 (c), RuO_x-MIL-125(Ti)-NH_2 (d) and Pt-RuO_x-MIL-125(Ti)-NH_2 (e) at 21 h reaction time. Reaction conditions: Photocatalyst (20 mg /20 mL Milli Q-H_2O), UV-Vis Xe lamp (150 $mW \times cm^{-2}$), temperature 35 ˚C.

As it has been already remarked, the MIL-125(Ti)-NH_2 photocatalysts do not contain exactly the same co-catalyst loading (Table 1). Thus, although the initial particle size was similar for all the samples, due to the intrinsic conditions of the photodeposition method, loading was somewhat different. Therefore, it could be that the photocatalytic efficiency varied somewhat as a function of the co-catalyst loading. To take into account the co-catalyst loading as a possible parameter, the experimental gas evolution rates were divided by the mass of the co-catalyst, rather than by the mass of MIL-125(Ti)-NH_2. The results are presented in Figure 6.

As it can be seen in this Figure, plotting the data in this way shows that Pt is RuO_x a somewhat better co-catalyst per mass unit than CoO_x, although the activity when a single co-catalyst is present varies in a relatively small range. In addition, this plot also shows the benefits of having two complementary co-catalysts for the overall water splitting, since the activity of Pt-RuO_x-MIL-125(Ti)-NH_2 increases by a higher factor of about three with respect to the improvement when a single co-catalyst is present.

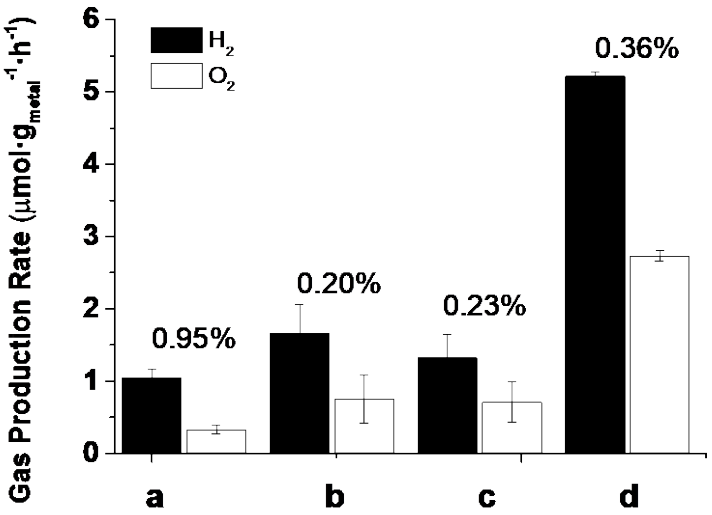

Figure 6. H_2 and O_2 maximum production rates. Production rate in mmol per gram of deposited metal co-catalyst per hour. Legend: CoO_x-MIL-125(Ti)-NH_2 (a), Pt-MIL-125(Ti)-NH_2 (b), RuO_x-MIL-125(Ti)-NH_2 (c) and Pt-RuO_x-MIL-125(Ti)-NH_2 (d). The number represents the metal weight percent supported in the MOF. Reaction conditions: Photocatalysts (20 mg /20 mL Milli Q-H_2O), UV-Vis Xe lamp (150 mW×cm^{-2}), temperature 35 ˚C, reaction time: 6 h.

The stability of the used catalyst after 22 h irradiation were evaluated by their characterization by PXRD and TEM measurements. Importantly, it should be commented that all the tested photocatalysts for the overall water splitting retains their initial crystallinity as revealed by XRD measurements (Figures S17-S21). TEM measurements reveal that the average particle size of the supported NPs on the MIL-125(Ti)-NH2 after 22 h irradiation during the photocatlytic experiment (Figure S22) only slightly increases (<0.2 nm in average) respect to the fresh samples, possibly due to the operation of the Ostwald ripening mechanism during the photocatalytic reaction. XPS of the most active sample Pt-RuOx-MIL-125(Ti)-NH_2 after one

use further confirms the stability of this photocatalyst under the present reaction conditions (Figure S23).

One of the challenges in photocatalysis for the overall water splitting is develop efficient materials under visible light irradiation. Importantly, the most active Pt-RuO_x-MIL-125(Ti)-NH_2 photocatalyst prepared in this work is able to use the natural Sunlight irradiation to promote the overall water splitting. Results show that under natural sunlight irradiation Pt-RuO_x-MIL-125(Ti)-NH_2 was able to achieve the overall water splitting with a maximum production of 27 $\mu mol \cdot g^{-1}$ of H_2 and 14 $\mu mol \cdot g^{-1}$ of O_2 (Figure 7a). This is one of the first examples in which a MOF material has demostrated their ability to perform the quasi-stoichiometric overall water splitting under real conditions.

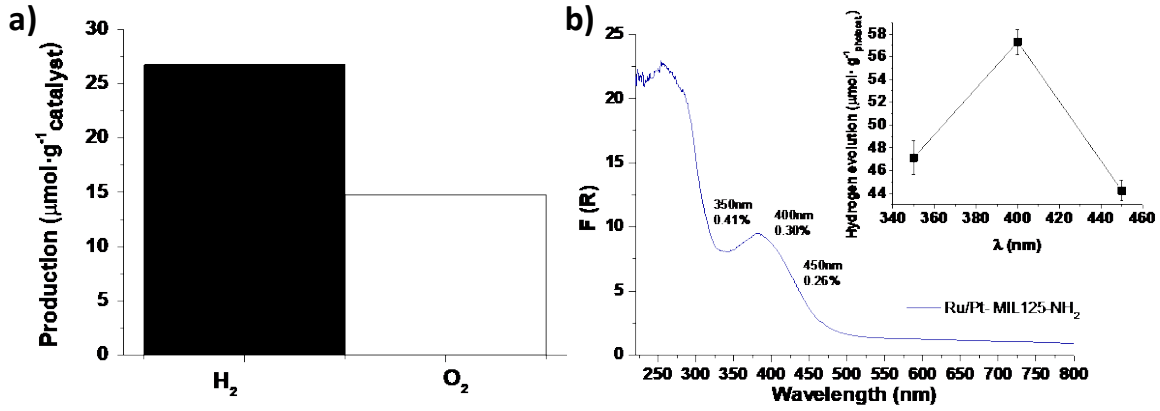

Figure 7. a) Photocatalytic overall water splitting under natural Sunlight irradiation using Pt-RuOx-MIL-125(Ti)-NH_2. Reaction conditions: Photocatalyst (20 mg/20 mL Milli Q-H_2O), sunlight (100 $mW \times cm^{-2}$), ambient temperature 30 ˚C, reaction time: 10h. b) H_2 production using a monochromator at the selected wavelengths and comparison in the UV-Vis spectra. Reaction conditions: Photocatalyst (20 mg /20 mL Milli Q-H_2O), sample was irradiated using a 150W Xenon lamp equipped with a CzernveTurner monochromator, temperature (35 ˚C), reaction time: 21h.

Using the most efficient Pt-RuO_2-MIL-125(Ti)-NH_2 photocatalyst the quantum efficiency at selected wavelengths was determined by using monochromatic light. As it can be seen in Figure 7b, the photocatalytic activity data follows the absorption spectrum of the material, being the efficiency at 400 nm higher than at 350 nm or 450 nm. The maximum

quantum efficiency for overall water splitting is remarkable and ranks Pt-RuO_2-MIL-125(Ti)-NH_2 among the most efficient photocatalysts reported so far.

As observed in the results commented earlier, the fact that H_2 and O_2 are stoichiometrically produced, suggests that gases evolution arises from water splitting reaction. To further investigate this fact, an experiment was designed where isotopically labeled $H_2{}^{18}O$ was utilized (97 atom % ^{18}O normalized with respect to hydrogen) instead of regular water. The evolution of the isotopically labelled O_2 (36 m/z) was followed by gas chromatography mass spectrometry (GC/MS), as well as the possible molecule fragmentation usually observed in this technique. In this case the reaction was purged with helium to avoid the presence of argon since the latter exhibits the ^{36}Ar stable isotope occurring with a natural abundance of 0.337%. Table 3 summarizes the m/z ratio abundance obtained for the different masses. The peak corresponding to 36 m/z shows a three fold increase after 24 hours of light radiation (up to 0.32%) (Figure S24). Another remarkable change is the approximately twenty fold enhancement in the signal corresponding to the 18 m/z with respect to sample taken before reaction owing to the oxygen molecule (^{18}O-^{18}O) fragmentation during the analysis, values from 0.45% before irradiation to 8.5% after 24h. All the evidences commented above lead to the conclusion that the overall water splitting reaction is photocatalized by the metal organic framework and that the oxygen generated in the reaction comes from the water added in the reaction.

Table 3. % Abundance for the different m/z ratio elements found by mass spectrometry during the course of the reaction (normalized to the peak of 32).

m/z ratio [% abundance]	**36**	34	20	**18**	16
0 h	**0.11**	0.6	2.1	**0.45**	5.5
24 h	**0.32**	0.38	1.5	**8.5**	5.9

4. Conclusions

In the present work it has been found that MIL-125(Ti)-NH_2 as photocatalyst can promote overall water splitting evolving H_2 and O_2 in the expected stoichiometric amounts. The activity of this material is strongly dependent on the presence and nature of co-catalysts. Although photodeposition method has the advantage that locates the co-catalyst NPs at the places in the crystal where electrons are holes are present, the exact loading amount of co-catalyst cannot be controlled. When corrected for the co-catalyst mass, it has been determined that the activity enhancement follows the order: $Pt \approx RuO_2 > CoO_x$. The presence of complementary co-catalysts increases even further the activity that has reached a maximum hydrogen production of 218 $\mu mol \times g^{-1}$, with a maximum quantum efficiency at 400 nm of 0.30.

Acknowledgements

Financial support by the Spanish Ministry of Economy and Competitiveness [Severo Ochoa and CTQ2015-69163-CO2-R1] and Generalitat Valenciana [Prometeo 2017-083] is gratefully acknowledged. S.R.-B. also thanks the Research Executive Agency (REA) and the European Commission, for the funding received under the Marie Skłodowska-Curie actions [H2020-MSCA-IF-2015/ Grant agreement number 709023/ ZESMO]. S.N. thanks financial support by the Fundación Ramón Areces (XVIII Concurso Nacional para la Adjudicación de Ayudas a la Investigación en Ciencias de la Vida y de la Materia, 2016).

Appendix A. Supplementary Data

Supplementary material related to this article can be found, in the online version, at doi:

($^{\perp}$ S.R.-B. and M. C. contributed equally in the experimental part of this work)

Titanium containing metal organic framework conveniently modified by inclusion co-catalysts can promote the photocatalytic generation of H_2 and O_2 (218 and 85 $\mu mol \cdot g_{photocatalyst}^{-1}$, respectively, at 24 h) from H_2O.

Keywords: heterogeneous photocatalysis; metal-organic frameworks: MIL-125(Ti)-NH_2; metal nanoparticles; overall water splitting

Sonia Remiro-Buenamañana[1,*] María Cabrero,[2] Marcos Martínez-Guanter,[1] Mercedes Álvaro,[2] Sergio Navalón,[2,*] Hermenegildo García[1,2,3,*]

Influence of co-catalysts on the photocatalytic activity of MIL-125(Ti)-NH_2 in the overall water splitting

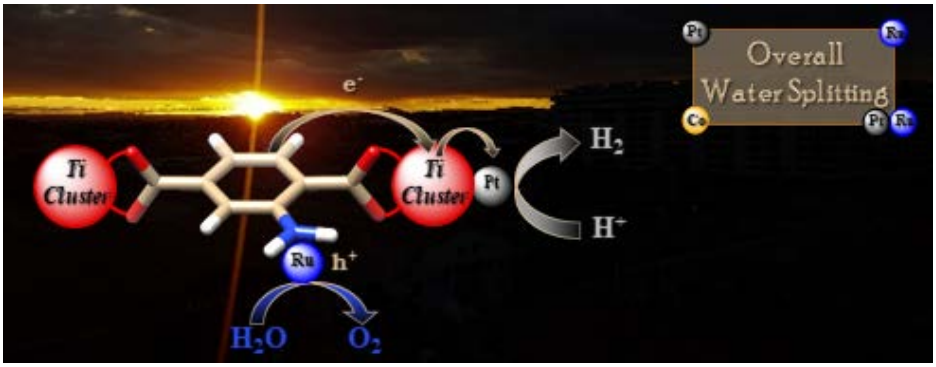

1. Gust, D.; Moore, T. A.; Moore, A. L., *Acc. Chem. Res.* **2009,** *42* (12), 1890-1898.
2. Centi, G.; Perathoner, S., *ChemSusChem.* **2010,** *3* (2), 195-208.
3. Gray, H. B., *Nat. Chem.* **2009,** *1* (1), 7.
4. Li, K.; Peng, B.; Peng, T., *ACS Catal.* **2016,** *6* (11), 7485-7527.
5. Kamat, P. V.; Bisquert, J., Solar fuels. Photocatalytic hydrogen generation. ACS Publications: 2013.
6. Li, J.; Wu, N., *Catal. Sci. Technol.* **2015,** *5* (3), 1360-1384.
7. Protti, S.; Albini, A.; Serpone, N., *PCCP* **2014,** *16* (37), 19790-19827.
8. Ni, M.; Leung, M. K.; Leung, D. Y.; Sumathy, K., *Renew. Sust. Energ. Rev.* **2007,** *11* (3), 401-425.
9. Fujishima, A.; Rao, T. N.; Tryk, D. A., *J. Photoch. Photobio. C* **2000,** *1* (1), 1-21.
10. Malato, S.; Blanco, J.; Vidal, A.; Richter, C., *Appl. Catal. B* **2002,** *37* (1), 1-15.
11. Li, Y.; Xu, H.; Ouyang, S.; Ye, J., *PCCP* **2016,** *18* (11), 7563-7572.
12. Zhang, T.; Lin, W., *Chem. Soc. Rev.* **2014,** *43* (16), 5982-5993.
13. Wang, J.-L.; Wang, C.; Lin, W., *ACS Catal.* **2012,** *2* (12), 2630-2640.
14. Dhakshinamoorthy, A.; Asiri, A. M.; Garcia, H., *Angew. Chem. Int. Ed.* **2016,** *55* (18), 5414-5445.
15. Dhakshinamoorthy, A.; Li, Z.; Garcia, H., *Chem. Soc. Rev.* **2018**.
16. Rowsell, J. L.; Yaghi, O. M., *Microporous Mesoporous Mater.* **2004,** *73* (1-2), 3-14.
17. Long, J. R.; Yaghi, O. M., *Chem. Soc. Rev.* **2009,** *38* (5), 1213-1214.
18. Lee, J.; Farha, O. K.; Roberts, J.; Scheidt, K. A.; Nguyen, S. T.; Hupp, J. T., *Chem. Soc. Rev.* **2009,** *38* (5), 1450-1459.
19. Matsuda, R.; Kitaura, R.; Kitagawa, S.; Kubota, Y.; Belosludov, R. V.; Kobayashi, T. C.; Sakamoto, H.; Chiba, T.; Takata, M.; Kawazoe, Y., *Nature* **2005,** *436* (7048), 238.
20. Cheetham, A. K.; Férey, G.; Loiseau, T., *Angew. Chem. Int. Ed.* **1999,** *38* (22), 3268-3292.
21. Li, H.; Eddaoudi, M.; O'Keeffe, M.; Yaghi, O. M., *nature* **1999,** *402* (6759), 276.
22. Gomes Silva, C.; Luz, I.; Llabrés i Xamena, F. X.; Corma, A.; García, H., *Chemistry–A European Journal* **2010,** *16* (36), 11133-11138.
23. Horiuchi, Y.; Toyao, T.; Saito, M.; Mochizuki, K.; Iwata, M.; Higashimura, H.; Anpo, M.; Matsuoka, M., *J. Phys. Chem. C* **2012,** *116* (39), 20848-20853.
24. Hendon, C. H.; Tiana, D.; Fontecave, M.; Sanchez, C. m.; D'arras, L.; Sassoye, C.; Rozes, L.; Mellot-Draznieks, C.; Walsh, A., *J. Am. Chem. Soc.* **2013,** *135* (30), 10942-10945.
25. Alvaro, M.; Carbonell, E.; Ferrer, B.; Llabres i Xamena, F. X.; Garcia, H., *Chemistry–A European Journal* **2007,** *13* (18), 5106-5112.
26. Xiao, J. D.; Shang, Q.; Xiong, Y.; Zhang, Q.; Luo, Y.; Yu, S. H.; Jiang, H. L., *Angew. Chem. Int. Ed.* **2016,** *55* (32), 9389-9393.
27. Fu, Y.; Sun, D.; Chen, Y.; Huang, R.; Ding, Z.; Fu, X.; Li, Z., *Angew. Chem. Int. Ed.* **2012,** *51* (14), 3364-3367.
28. Sun, D.; Fu, Y.; Liu, W.; Ye, L.; Wang, D.; Yang, L.; Fu, X.; Li, Z., *Chemistry–A European Journal* **2013,** *19* (42), 14279-14285.
29. Chen, X.; Shen, S.; Guo, L.; Mao, S. S., *Chem. Rev.* **2010,** *110* (11), 6503-6570.
30. Gomes Silva, C. u.; Juárez, R.; Marino, T.; Molinari, R.; García, H., *J. Am. Chem. Soc.* **2010,** *133* (3), 595-602.
31. Maeda, K.; Xiong, A.; Yoshinaga, T.; Ikeda, T.; Sakamoto, N.; Hisatomi, T.; Takashima, M.; Lu, D.; Kanehara, M.; Setoyama, T., *Angew. Chem.* **2010,** *122* (24), 4190-4193.
32. Silva, C. G.; Bouizi, Y.; Fornés, V.; García, H., *J. Am. Chem. Soc.* **2009,** *131* (38), 13833-13839.
33. Meyer, K.; Ranocchiari, M.; van Bokhoven, J. A., *Energ. Environ. Sci.* **2015,** *8* (7), 1923-1937.

34. An, Y.; Xu, B.; Liu, Y.; Wang, Z.; Wang, P.; Dai, Y.; Qin, X.; Zhang, X.; Huang, B., *ChemistryOpen* **2017,** *6* (6), 701-705.
35. An, Y.; Liu, Y.; An, P.; Dong, J.; Xu, B.; Dai, Y.; Qin, X.; Zhang, X.; Whangbo, M. H.; Huang, B., *Angew. Chem. Int. Ed.* **2017,** *56* (11), 3036-3040.
36. Nasalevich, M. A.; Hendon, C. H.; Santaclara, J. G.; Svane, K.; van der Linden, B.; Veber, S. L.; Fedin, M. V.; Houtepen, A. J.; van der Veen, M. A.; Walsh, A.; Gascon, J., *Sci. Rep* **2016,** *6*.
37. Moreira, M. A.; Santos, J. C.; Ferreira, A. F. P.; Loureiro, J. M.; Ragon, F.; Horcajada, P.; Yot, P. G.; Serre, C.; Rodrigues, A. E., *Microporous Mesoporous Mater.* **2012,** *158*, 229-234.
38. Daliran, S.; Santiago-Portillo, A.; Navalón, S.; Oveisi, A. R.; Álvaro, M.; Ghorbani-Vaghei, R.; Azarifar, D.; García, H., *J. Colloid Interface Sci.* **2018,** *532*, 700-710.
39. Dan-Hardi, M.; Serre, C.; Frot, T.; Rozes, L.; Maurin, G.; Sanchez, C.; Férey, G., *J. Am. Chem. Soc.* **2009,** *131* (31), 10857-10859.
40. Wenderich, K.; Mul, G., *Chem. Rev.* **2016,** *116* (23), 14587-14619.
41. Vaesen, S.; Guillerm, V.; Yang, Q.; Wiersum, A. D.; Marszalek, B.; Gil, B.; Vimont, A.; Daturi, M.; Devic, T.; Llewellyn, P. L.; Serre, C.; Maurin, G.; De Weireld, G., *Chem. Commun.* **2013,** *49* (86), 10082-10084.
42. Wang, H.; Yuan, X.; Wu, Y.; Zeng, G.; Chen, X.; Leng, L.; Wu, Z.; Jiang, L.; Li, H., *J. Hazard. Mater.* **2015,** *286*, 187-194.
43. Zhang, L.; Cui, P.; Yang, H.; Chen, J.; Xiao, F.; Guo, Y.; Liu, Y.; Zhang, W.; Huo, F.; Liu, B., *Adv. Sci.* **2016,** *3* (1), 1500243.
44. Nasalevich, M. A.; Hendon, C. H.; Santaclara, J. G.; Svane, K.; Van Der Linden, B.; Veber, S. L.; Fedin, M. V.; Houtepen, A. J.; Van Der Veen, M. A.; Kapteijn, F., *Sci. Rep* **2016,** *6*, 23676.
45. de Miguel, M.; Ragon, F.; Devic, T.; Serre, C.; Horcajada, P.; García, H., *ChemPhysChem* **2012,** *13* (16), 3651-3654.
46. Nasalevich, M. A.; Becker, R.; Ramos-Fernandez, E. V.; Castellanos, S.; Veber, S. L.; Fedin, M. V.; Kapteijn, F.; Reek, J. N. H.; van der Vlugt, J. I.; Gascon, J., *Energ. Environ. Sci.* **2015,** *8* (1), 364-375.
47. Hendon, C. H.; Tiana, D.; Fontecave, M.; Sanchez, C.; D'arras, L.; Sassoye, C.; Rozes, L.; Mellot-Draznieks, C.; Walsh, A., *J. Am. Chem. Soc.* **2013,** *135* (30), 10942-10945.
48. Zhu, B.; Zou, R.; Xu, Q., *Adv. Energy. Mater.* **2018,** *8* (24), 1801193.
49. Kampouri, S.; Nguyen, T. N.; Ireland, C. P.; Valizadeh, B.; Ebrahim, F. M.; Capano, G.; Ongari, D.; Mace, A.; Guijarro, N.; Sivula, K.; Sienkiewicz, A.; Forro, L.; Smit, B.; Stylianou, K. C., *J. Mater. Chem. A* **2018,** *6* (6), 2476-2481.
50. Yang, J.; Wang, D.; Han, H.; Li, C., *Acc. Chem. Res.* **2013,** *46* (8), 1900-1909.
51. Han, J.; Wang, D.; Du, Y.; Xi, S.; Hong, J.; Yin, S.; Chen, Z.; Zhou, T.; Xu, R., *J. Mater. Chem. A* **2015,** *3* (41), 20607-20613.
52. Bamwenda, G. R.; Uesigi, T.; Abe, Y.; Sayama, K.; Arakawa, H., *Appl. Catal. A-Gen.* **2001,** *205* (1), 117-128.